

Large-scale spatiotemporal patterns in a ring of nonlocally coupled oscillators with a repulsive coupling

Bojun Li  and Nariya Uchida ^{*}

Department of Physics, Tohoku University, Sendai 980-8578, Japan

 (Received 30 July 2021; revised 21 October 2021; accepted 8 November 2021; published 22 November 2021)

Nonlocally coupled oscillators with a phase lag exhibit various nontrivial spatiotemporal patterns such as the chimera states and the multitwisted states. We numerically study large-scale spatiotemporal patterns in a ring of oscillators with a repulsive coupling with a phase delay parameter α . We find that the multichimera state disappears when α exceeds a critical value. Analysis of the fraction of incoherent regions shows that the transition is analogous to that of directed percolation with two absorbing states but that their critical behaviors are different. The multichimera state reappears when α is further increased, exhibiting nontrivial spatiotemporal patterns with a plateau in the fraction of incoherent regions. A transition from the multichimera to multitwisted states follows at a larger value of α , resulting in five collective phases in total.

DOI: [10.1103/PhysRevE.104.054210](https://doi.org/10.1103/PhysRevE.104.054210)

I. INTRODUCTION

The collective behavior of coupled oscillators is ubiquitous in nature [1,2]. When the coupling is weak, the dynamics of oscillators are described only by a phase parameter by means of phase reduction. Depending on the form of the coupling function, the phase oscillators exhibit not only global synchronization and desynchronization [3] but also spatial coexistence of coherent and incoherent regions known as the chimera states [4–6]. Originally found in nonlocally coupled oscillators on a one-dimensional ring, the chimera states are observed also in two or three dimensions [7–10], and in globally [11–13] or locally [14,15] coupled oscillator systems. They are experimentally realized in chemically [16–18], mechanically [19,20], and electronically [21,22] coupled oscillators, and also attracting attention in terms of neuronal networks [23,24]. A widely used model to study the chimera states is the nonlocally coupled phase oscillators on a ring, the time evolution of which obeys

$$\dot{\psi}(x, t) = \omega_0 - \frac{1}{2R} \sum_{\substack{y=x-R \\ y \neq x}}^{x+R} \sin[\psi(x, t) - \psi(y, t) + \alpha\pi], \quad (1)$$

where $\psi(x, t)$ represents the phase of the oscillator at $x = 1, 2, \dots, N$ at time t , R is the coupling range, and $\alpha\pi$ gives the phase lag. The intrinsic phase velocity ω_0 is constant and set to zero without losing generality by the transformation $\psi \rightarrow \psi - \omega_0 t$. Therefore, the spatiotemporal patterns are predominantly determined by α and $r = R/N$. For a pair of oscillators, the phase lag α causes in-phase synchronization for $|\alpha| < 1/2$ (attractive coupling) and antiphase synchronization for $1/2 < |\alpha| \leq 1$ (repulsive coupling). For three or more oscillators, the phase lag introduces frustration and causes nonuniform patterns of synchronization. Previous studies on

the chimera and twisted states focused mostly on the case $r \approx 10^{-1}$, where a single or a small number of incoherent clusters appear. Recent studies on a large system ($r \ll 1$) with attractive coupling [25,26] found randomly branching patterns of many clusters that resemble the patterns in directed percolation (DP). DP is a two-state model of nonequilibrium critical phenomena and describes the onset of turbulence in fluid systems [27–29]. In terms of the chimera states, the coherent and incoherent sites correspond to inactive and active sites in DP, respectively. The aim of the present paper is to extend the analogy to repulsive coupling and to explore novel multicluster patterns beyond the analogy.

The collective behavior of the oscillator system governed by Eq. (1) is summarized as follows: For $\alpha = 0$ and $R > R_c \approx 0.34N$, a uniformly synchronized state is the only stable state [30]. For $R < R_c$, the traveling-wave solution

$$\psi(x, t) = \Omega t + Qx, \quad Q = \frac{2\pi q}{N}, \quad (2)$$

where q is an integer with $|q| \leq \frac{N-1}{2}$, also becomes stable. This state is called the q -twisted state [30]. The uniform and q -twisted states are replaced by the chimera states as α is increased and approaches $\frac{1}{2}$ [8,31,32]. If the coupling range is sufficiently small compared with the system size, the multichimera states with many coherent and incoherent domains are obtained. For $\alpha = 1$, a q -twisted state or coexistence of multiple q -twisted states (multitwisted states) are obtained [33]. As α is decreased from 1, chimera states appear from the multitwisted state and the number of incoherent regions grows. Three scenarios for the chimera birth have been reported [34].

In this paper, we study the statistical properties of system (1) for a repulsive coupling ($\frac{1}{2} < \alpha < 1$) and $R \ll N$, exploiting an analogy to directed percolation with two symmetric absorbing states (DP2) [35]. In directed percolation, active (percolated) states propagate to neighbor sites with probability p and form randomly branching patterns [36]. Once the propagation stops, the active sites will not be generated

^{*}uchida@cmpt.phys.tohoku.ac.jp

from the inactive sites. Therefore, the inactive state is called an absorbing state. The fraction of active sites ρ_{DP} shows a critical behavior $\rho_{\text{DP}} \sim (p - p_c)^{\beta_{\text{DP}}}$ in the dynamical steady states. In DP2, there are two inactive states I_1 and I_2 that are symmetric in their time evolution rules. The active sites form domain walls between the two types of inactive domains. The domain walls fluctuate until they collide and annihilate mutually, resulting in algebraic decay of their fraction $\rho_{\text{wall}} \propto t^{-1/2}$ [35,36]. In one dimension, the active sites are interpreted as diffusing particles which annihilate by reaction $2A \rightarrow \emptyset$ and is generated by an offspring production $A \rightarrow 3A$. In the present model, the q -twisted states with $q > 0$ and $q < 0$ correspond to the two absorbing states, and the transition region between the two q -twisted region corresponds to the active site in DP2. We find a transition from multichimera state to a twisted state at a critical point α_c as we increase α from $\frac{1}{2}$ and compare the critical behavior with that of DP2. Further increasing α , the multichimera state reappears with nontrivial spatiotemporal patterns. The fraction of incoherent sites shows a nonmonotonic dependence on α , and we classify the spatial-temporal patterns into five phases.

II. LINEAR STABILITY ANALYSIS

In this section, we briefly recapitulate the linear stability analysis of the q -twisted states, which has been done for $\alpha = \pi$ in Ref. [33] and for general α and finite N in Ref. [37]. Here we consider the case of general α in the continuum limit $N \rightarrow \infty$, by adding a small perturbation to the solution for the q -twisted state as

$$\psi(x, t) = \Omega t + Qx + \sum_K A_K e^{iKx + \Lambda_K t}. \quad (3)$$

Here $A_K (\ll 1)$ and Λ_K are the amplitude and growth rate of the mode with the wave number $K = 2\pi k/N$, respectively, and the sum is taken over $k = 1, 2, \dots, N-1$. Substituting this solution into the governing equation (1) and linearizing it with respect to A_K , we get

$$\Omega = -\frac{1}{2R} \sum_{\substack{s=-R \\ s \neq 0}}^R \sin(-Qs + \alpha\pi) \quad (4)$$

at the zeroth order and

$$\begin{aligned} \sum_K \Lambda_K A_K e^{iKx + \Lambda_K t} &= -\frac{1}{2R} \sum_{\substack{s=-R \\ s \neq 0}}^R \cos(-Qs + \alpha\pi) \\ &\times \sum_K A_K e^{iKx + \Lambda_K t} (1 - e^{iKs}) \end{aligned} \quad (5)$$

at the first order, where $s = y - x$. From Eq. (5), we extract the linear growth rate of the perturbation as

$$\text{Re } \Lambda_K = -\frac{1}{2R} \cos \alpha\pi \sum_{\substack{s=-R \\ s \neq 0}}^R \cos Qs (1 - \cos Ks). \quad (6)$$

Note that the sign of $\text{Re } \Lambda_K$ does not depend on α for $\frac{1}{2} < \alpha \leq 1$. We plot the normalized growth rate $\text{Re } \Lambda_K / (-\cos \alpha\pi)$ as a function of Q and K and for $R = 5$ in Fig. 1(a). The q -twisted

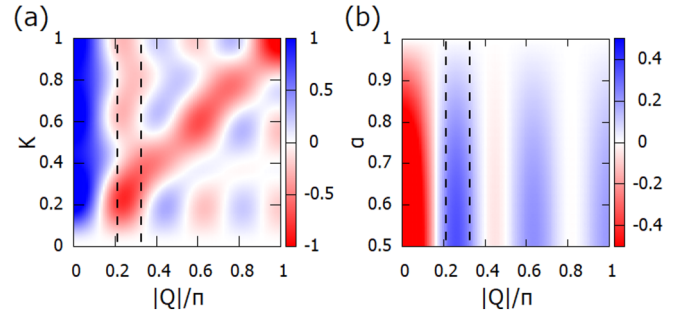


FIG. 1. (a) The normalized linear growth rate $\text{Re } \Lambda_K / |\cos \alpha\pi|$ given by Eq. (6), for $R = 5$ and $\frac{1}{2} < \alpha \leq 1$ as a function of K and $|Q|/\pi$. (b) The phase velocity of the q -twisted state given by Eq. (4) for $R = 5$ as a function of α and $|Q|/\pi$. In both plots, the borders of the linearly stable range $0.215 < |Q|/\pi < 0.323$ are shown by dotted lines.

state with $Q = 2\pi q/N$ is stable if $\text{Re } \Lambda_K < 0$ for $0 < K < 1$. The stable range is approximately given by $0.215\pi < Q < 0.323\pi$, which coincides with the previous result for $\alpha = 1$ [33]. Note also that the stability range is extended for finite N because the condition for stability is $\text{Re } \Lambda_K < 0$ for a finite number of K [37]. The phase velocity Ω of an unperturbed q -twisted state for $R = 5$ is plotted in Fig. 1(b). Its sign changes three times as the wave number Q is increased and is positive in the linearly stable range. The absolute value of Ω converges to zero as α approaches 1. The stable range is narrowed as we increase R [33,37], which is interpreted as the result of frustration between many oscillators. From the observation that the linearly stable range roughly corresponds to a band of positive phase velocity, we can relate the stability to the sum in Eq. (4), which approaches zero as R is increased. Thus the existence of stable twisted states is a consequence of the finite interaction range.

III. SIMULATION RESULT

A. Spatiotemporal patterns

We solved Eq. (1) with $\omega_0 = 0$ and $R = 5$ for $N = 10000$ using the Runge-Kutta method with the time step $\Delta t = 0.01$. The initial phases are randomly distributed in $(-\pi : \pi]$, and the periodic boundary condition is applied. In Fig. 2, we show typical spatial profiles of the phase difference of neighbor oscillators,

$$\Delta(x, t) = \frac{\psi(x+1, t) - \psi(x, t)}{\pi} \in (-1 : 1], \quad (7)$$

and the normalized frequency distribution of Δ .

When $\alpha = 0.5$, the phases of oscillators are distributed uniformly, and so are their phase differences [Figs. 2(a) and 2(b)]. As α is increased, a chimera state consisting of twisted and incoherent regions appears [Fig. 2(c)]. Two kind of twisted regions with positive or negative phase differences appear alternatively with an incoherent region in between. The distribution of Δ has double peaks in the linearly stable range obtained in Sec. II [Fig. 2(d)]. As α is further increased, the twisted regions become larger and the distribution of Δ becomes sharper [Figs. 2(e)–2(h)]. The spatial profile of Δ in the incoherent region is oscillatory, and convergence to the

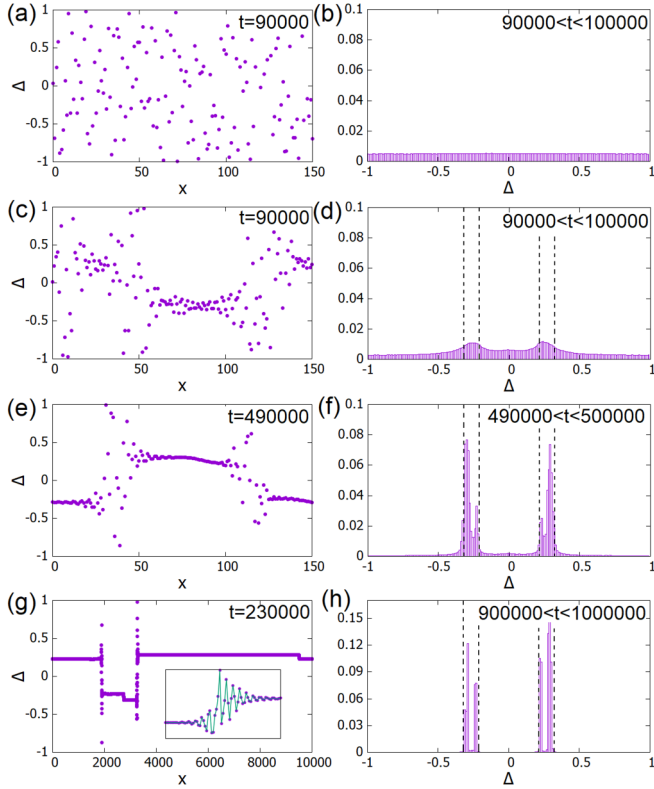


FIG. 2. Spatial profiles (left) and histogram (right) of $\Delta(x)$ for (a), (b) $\alpha = 0.5$; (c), (d) $\alpha = 0.65$; (e), (f) $\alpha = 0.70$; and (g), (h) $\alpha = 0.73$. The plots in panels (a), (c), (e) show only 150 of the 10 000 oscillators. Panel (g) shows the whole system and a magnified view of the border between two twisted regions (inset). The dotted lines in the histograms (d), (f), and (h) show the borders of the linearly stable range $0.215 < |\Delta| < 0.323$.

stable value in the twisted region looks similar to the Gibbs phenomenon in Fourier series [Fig. 2(h), inset].

The spatiotemporal pattern of $\Delta(x, t)$ is shown in Figs. 3(a)–3(k). The positively and negatively twisted regions are separated by narrow incoherent regions, and offspring-production and pair-annihilation of incoherent regions (separation and coalescence of twisted regions) are observed.

To exploit the analogy with directed percolation, we distinguish the twisted sites and incoherent sites by using the local standard deviation of phase difference,

$$\sigma_{\Delta}(x, t) = \sqrt{\frac{1}{2R} \sum_{y=x-R}^{x+R-1} [\Delta(y, t) - \bar{\Delta}]^2}. \quad (8)$$

If $\sigma_{\Delta}(x) < \sigma_c$, the site x is defined as twisted, and if $\sigma_{\Delta}(x) > \sigma_c$ the site x is incoherent. We choose $\sigma_c = 0.1$ which roughly matches with the width of the linearly stable range of the phase difference. We define the state variable $s(x, t) = \pm 1$ for a site with a positive and negative phase difference, respectively, and $s(x, t) = 0$ for an incoherent site. A sample of the spatiotemporal patterns of $s(x, t)$ is shown Fig. 3(l). Interestingly, in addition to pair production and annihilation of the incoherent regions, we find branching of one incoherent region into two and merger of two incoherent regions into one.

In these cases, one of the incoherent region is sandwiched by twisted regions with Δ of the same sign. This is a difference from DP2, in which each active site is always located between different inactive states.

The fraction of incoherent sites is defined by [38]

$$\rho(t) = \frac{1}{N} \sum_{x=1}^N [1 - s(x, t)^2]. \quad (9)$$

For each simulation, $\rho(t)$ either decays to zero or fluctuates around a constant value after a sufficiently long time depending on α and the initial condition.

B. Absorbing-state transition

For $\alpha < 0.79$, the spatiotemporal patterns [Figs. 3(a)–3(e)] resemble those in DP2 that the twisted (inactive) regions grow in size and the irregularly fluctuating incoherent (active) region diminishes as α is increased. The time evolution of $\rho(t)$ for $0.70 \leq \alpha \leq 0.78$ is shown in Figs. 4(a) and 4(b). We take the time-average over the late stage and ensemble average for each α to define the asymptotic value $\rho_{\infty} = \rho_{\infty}(\alpha)$. The plots of the stationary fraction $\rho_{\infty}(\alpha)$ in Figs. 4(c) and 4(d) show that ρ_{∞} decreases to zero as α approaches $\alpha_c = 0.722$. Fitting by the power law $\rho_{\infty} \sim |\alpha - \alpha_c|^{\beta}$, $\beta = 0.755 \pm 0.028$ is obtained [Fig. 4(c)]. We define the states for $\alpha < \alpha_c = 0.722$ as “phase I,” which corresponds to the active phase in DP2. For $\alpha_c \leq \alpha < 0.79$, the number of incoherent regions is either zero or a very small even number (usually two or four), since the process conserves the number of incoherent regions modulo two. We call this state “phase II.” If $\rho_{\infty} = 0$, the whole space is occupied by one of the twisted states which satisfy the definition of “absorbing,” since incoherent sites never emerge from a single twisted region. This corresponds to the inactive phase in DP2. For $\alpha_c \leq \alpha < 0.75$, $\rho(t)$ decayed to zero by $t = 5 \times 10^6$ in six out of seven samples we tested. The survival time of the incoherent region varies. For $0.75 \leq \alpha \leq 0.78$, we tested 40 samples for $t < 5 \times 10^5$ and found that the time evolution of the incoherent fraction is fit by the power law $\rho(t) \sim t^{-\delta}$ with $\delta = 0.64 \pm 0.04$. We note that determination of the exponents β and δ with an accuracy of 0.1 requires the system size $N = 10^4$ or larger; finite-size effects make it impossible for $N = 10^3$ or less. This is because the incoherent fraction ρ changes discretely with the step size $\Delta\rho \sim 10R/N$ (if $R \ll N$), as each incoherent region has a width $\sim 5R$ and their number changes in pairs. [For example, a step of height $\Delta\rho \sim 0.005$ is seen in Fig. 4(a) for $\alpha = 0.74$ in the last stage of time evolution.] The step size is too large to approximate $\rho(t)$ and $\rho_{\infty}(\alpha)$ by smooth functions for $N = 10^3$ or less. Also, a small number of lingering incoherent regions in the phase II was observed only for the system size $N = 10^4$. For $N = 10^3$, all incoherent regions vanished within the simulation time. If two incoherent regions remain in the system, their lifetime is larger for a larger system as it takes more time for them to collide and annihilate. From the power-law decay of $\rho(t)$, we may argue that their lifetime is proportional to $N^{1/\delta}$ on average, but its variance was too large to determine the N dependence quantitatively.

The transition from the phase I to phase II is also reflected in the phase velocity $\dot{\psi}$. We show its average in Fig. 4(e) and

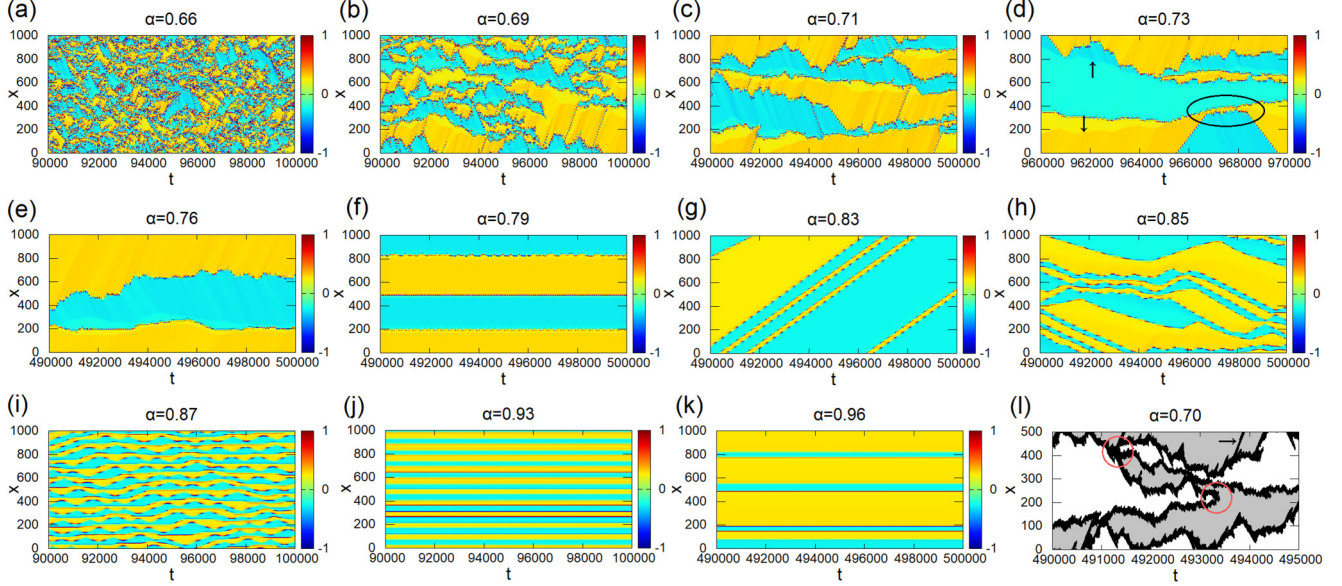


FIG. 3. (a)–(k) Spatiotemporal patterns of the phase difference $\Delta(x, t)$ for different values of α . Only 1000 out of 10 000 sites and a time window of width 10 000 are shown. Twisted regions with positive and negative phase difference are shown in yellow (light gray) and light blue (dark gray), and incoherent regions exist at the borders between them. In panel (d), the arrows show the boundaries between regions of slightly different Δ with the same sign. Two incoherent regions get close and are bounced back after a certain period of time are shown in the circle. (l) Spatiotemporal pattern of $s(x, t)$ for $\alpha = 0.70$. Black: $s = 0$ (incoherent). White and gray: $s = \pm 1$ (twisted). Pair-production and annihilation of incoherent sites are shown by red circles. Emission of a traveling wave is shown by an arrow.

its standard deviation σ_ω in Fig. 4(f), both as functions of α . The average phase velocity $\bar{\omega}$ is peaked at $\alpha = \alpha_c$, while σ_ω decays toward zero as the critical point is approached. For $\alpha > \alpha_c$, the standard deviation starts to rise again as $\rho_\infty(\alpha)$ does,

but vanishes again at $\alpha = 0.93$; see the next section for more details.

C. Resurgence of the multichimera states

For $\alpha \geq 0.79$, the spatiotemporal patterns of the phase difference changes dramatically [Figs. 3(f)–3(k)]. For statistical analysis of the patterns, we introduce the spatiotemporal correlation function of incoherent sites [38],

$$G(x, t) = \langle [1 - s(x', t')]^2 [1 - s(x' + x, t' + t)]^2 \rangle_{s(x', t')=0}. \quad (10)$$

It gives the conditional probability that $s(x' + x, t' + t) = 0$ under the condition that $s(x', t') = 0$. The space-time correlation function computed for the time window $90\,000 < t' < 100\,000$ is shown in Fig. 5. According to the behavior of $\rho_\infty(\alpha)$, $\sigma_\omega(\alpha)$, and $G(x, t)$, we classify the dynamics of system (1) for $\alpha \geq 0.79$ into the phases I to V. We also show spatiotemporal patterns of the phase velocity $\dot{\psi}(x, t)$ in Fig. 6, where some of the patterns of $\Delta(x, t)$ are also shown for comparison.

Unlike the behavior in the phases I and II, where the incoherent sites region diffuse from its original position [Figs. 5(a) and 6(a)], the incoherent region maintains a straight line for $\alpha = 0.79$ [Fig. 5(b)]. Phase III: for $0.80 \leq \alpha < 0.85$, the incoherent sites start to move at a constant speed at approximately 0.16 site per time unit [Figs. 5(c) and 6(b)]. The stationary fraction ρ_∞ increases with α to about 0.4. Phase IV: for $0.85 \leq \alpha < 0.93$, the system shows a novel spatiotemporal pattern of $\Delta(x, t)$ that consists of alternating straight lines and zigzag lines as shown in Fig. 6(c). The pattern of $\dot{\psi}(x, t)$ in the same region is shown in Fig. 6(d). We find a mesh-like pattern of small phase velocity. The moving direction of the

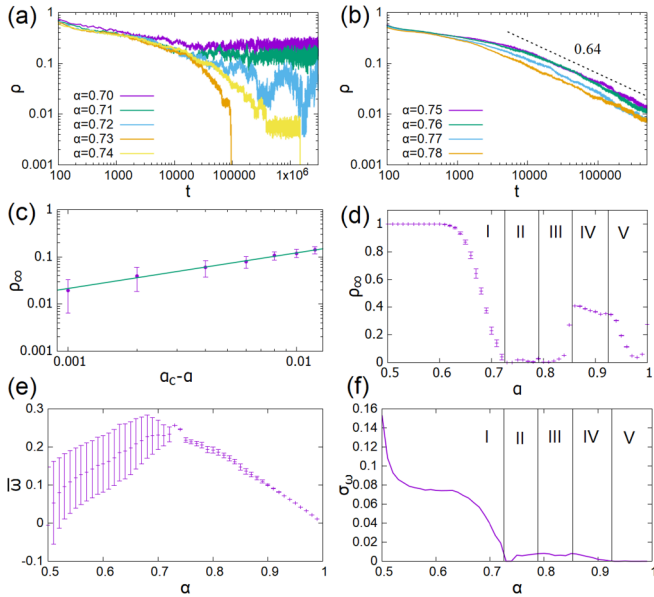


FIG. 4. (a), (b) Dependence of the incoherent fraction ρ on t . (c), (d) Dependence of ρ_∞ on α . The error bars show the standard deviation of $\rho(t)$ for (c) $t > 500\,000$, (d) $90\,000 < t < 100\,000$. (e) The average and (f) the standard deviation of the phase velocity. For $\alpha > 0.93$, the standard deviation of phase velocity becomes zero, which means the transition from the multichimera to the multitwisted state.

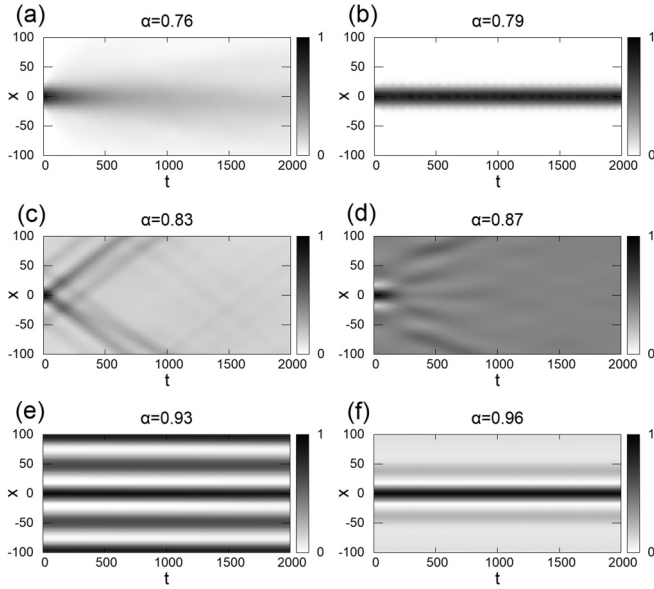


FIG. 5. The spatiotemporal correlation function $G(x, t)$. Gray scale represents the strength of correlation.

incoherent region is related to the phase velocity $\psi(x, t)$ of oscillators on each side. The zigzag-moving incoherent region always moves toward the side with smaller $\psi(x, t)$, while the $\psi(x, t)$ on each side of the straight line has the same value. For $\alpha = 0.91, 0.92$, the zigzag stripes begin to disappear which can be seen as a transition to the next phase. As seen in Fig. 4(f), the standard deviation of the phase velocity decreases to zero as we increase α and vanishes at $\alpha = 0.93$, Phase V: for $0.93 \leq \alpha < 1.00$, the whole system including the incoherent region between twisted regions evolves with the same phase velocity, as shown in Fig. 6(f), while the incoherent regions become straight in the spatiotemporal map

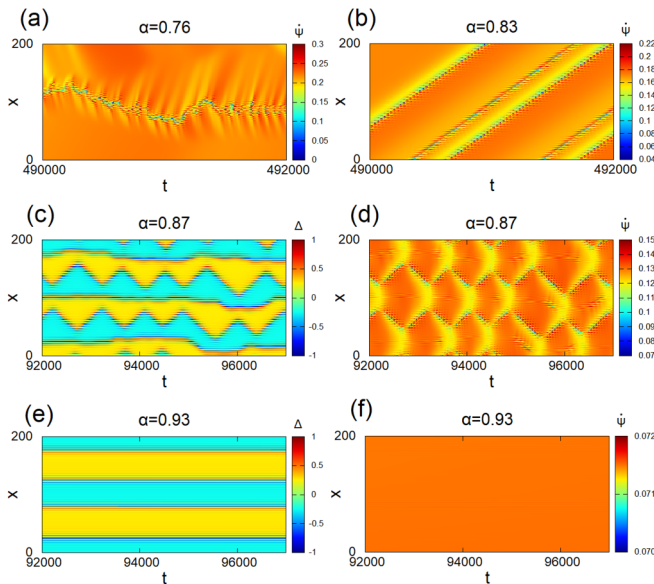


FIG. 6. The spatiotemporal pattern of the phase velocity $\psi(x, t)$ for (a) $\alpha = 0.78$, (b) 0.83 , (d) 0.87 , (f) 0.93 , and the phase difference $\Delta(x, t)$ for (c) $\alpha = 0.87$ and (e) 0.93 .

[Fig. 6(e)]. The transition from the phase IV to V accompanying uniformization of the phase velocity is found for a small number of clusters, and bifurcation scenarios are discussed [34]. By studying a large number of clusters, we find that the distances between incoherent regions become larger and lose its equality as α is increased, as seen in Figs. 5(e) and 5(f).

IV. DISCUSSION AND CONCLUSION

In summary, the spatiotemporal patterns of the nonlocally coupled oscillators are classified into five phases depending on the phase delay α . The transition from the phase I to II is qualitatively similar to the absorbing transition in DP2, in (i) pair production and annihilation of incoherent sites and (ii) vanishing of the incoherent fraction ρ_∞ at the critical point. The large system size allowed us to study the critical behavior with a sufficient accuracy to compare it with that of DP2. The critical exponent $\beta = 0.755 \pm 0.028$ is smaller than the corresponding exponent in DP2, $\beta_{DP} = 0.90$. Also, the exponent $\delta = 0.64 \pm 0.04$ characterizing the decay of $\rho(t)$ is larger than the DP2 value $\delta_{DP} = 0.5$. It shows that the irregular motion of incoherent regions is not described by a simple random walk as in DP2. These results lead us to the conclusion that the transition at $\alpha = \alpha_c$ does not belong to the DP2 universality class [35].

A possible origin of the deviation from DP2 is the existence of soliton-like traveling waves (narrow bands of incoherent sites emitted from incoherent regions) for $\alpha < \alpha_c$, such as those in Figs. 3(b), 3(c), and 3(l). For $\alpha_c < \alpha < 0.75$, we do not find soliton-like traveling waves but sometimes the incoherent region propagates at a constant speed, as seen in Fig. 3(d). The straight motion of incoherent regions enhances their collision and decay of the incoherent fraction $\rho(t)$. For $0.75 \leq \alpha < 0.79$, we find neither the traveling waves nor the straight motion, but the exponent $\delta > 1/2$ means that the trajectory of the incoherent region has long-time correlation and is not a simple random walk as in DP2. Another difference between DP2 and the coupled oscillators is that DP2 has only three possible states, whereas the wave number q in the oscillator system can take an arbitrary integer within the stable range. As a result, a single twisted region can contain different values of Δ . Boundaries between regions of slightly different values of Δ are seen in the profile at $x \approx 2800$ and 9500 in Fig. 2(g), and are also shown by arrows in Fig. 3(d). Such boundaries sometimes prevent pair annihilation of incoherent regions by repelling them back, as shown in the encircled region in Fig. 3(d). Quantitative analysis of the pair interaction and its effect on $\rho(t)$ is beyond the scope of this paper and left for future work.

For $\alpha > 0.79$, we find nonmonotonic change of the incoherent fraction and the spatiotemporal patterns are classified into the phases III to V. The nonmonotonic dependence as well as the zigzag pattern in the phase IV are highly nontrivial and the underlying mechanism needs clarification in future work.

ACKNOWLEDGMENT

We acknowledge financial support by JSPS KAKENHI Grant Number JP21K03396 to N.U.

- [1] A. Pikovsky, M. Rosenblum, and J. Kurths, *Synchronization: A Universal Concept in Nonlinear Sciences* (Cambridge University Press, Cambridge, 2001).
- [2] Y. Kuramoto, *Chemical Oscillations, Waves, and Turbulence* (Springer, Berlin, 1984).
- [3] J. A. Acebrón, L. L. Bonilla, C. J. Pérez Vicente, F. Ritort, and R. Spigler, *Rev. Mod. Phys.* **77**, 137 (2005).
- [4] Y. Kuramoto and D. Battogtokh, *Nonlinear Phenom. Complex Syst.* **5**, 380 (2002).
- [5] D. M. Abrams and S. H. Strogatz, *Phys. Rev. Lett.* **93**, 174102 (2004).
- [6] M. J. Panaggio and D. M. Abrams, *Nonlinearity* **28**, R67 (2015).
- [7] S.-i. Shima and Y. Kuramoto, *Phys. Rev. E* **69**, 036213 (2004).
- [8] P.-J. Kim, T.-W. Ko, H. Jeong, and H.-T. Moon, *Phys. Rev. E* **70**, 065201(R) (2004).
- [9] Y. Maistrenko, O. Sudakov, O. Osiv, and V. Maistrenko, *New J. Phys.* **17**, 073037 (2015).
- [10] E. Omel'chenko and E. Knobloch, *New J. Phys.* **21**, 093034 (2019).
- [11] A. Yeldesbay, A. Pikovsky, and M. Rosenblum, *Phys. Rev. Lett.* **112**, 144103 (2014).
- [12] V. K. Chandrasekar, R. Gopal, A. Venkatesan, and M. Lakshmanan, *Phys. Rev. E* **90**, 062913 (2014).
- [13] A. Mishra, C. Hens, M. Bose, P. K. Roy, and S. K. Dana, *Phys. Rev. E* **92**, 062920 (2015).
- [14] C. R. Laing, *Phys. Rev. E* **92**, 050904(R) (2015).
- [15] B. K. Bera and D. Ghosh, *Phys. Rev. E* **93**, 052223 (2016).
- [16] S. Nkomo, M. R. Tinsley, and K. Showalter, *Phys. Rev. Lett.* **110**, 244102 (2013).
- [17] J. F. Tetz, J. Rode, M. R. Tinsley, K. Showalter, and H. Engel, *Nat. Phys.* **14**, 282 (2018).
- [18] M. R. Tinsley, S. Nkomo, and K. Showalter, *Nat. Phys.* **8**, 662 (2012).
- [19] E. A. Martens, S. Thutupalli, A. Fourriere, and O. Hallatschek, *Proc. Natl. Acad. Sci. USA* **110**, 10563 (2013).
- [20] T. Kapitaniak, P. Kuzma, J. Wojewoda, K. Czolczynski, and Y. Maistrenko, *Sci. Rep.* **4**, 6379 (2014).
- [21] D. P. Rosin, D. Rontani, N. D. Haynes, E. Schöll, and D. J. Gauthier, *Phys. Rev. E* **90**, 030902(R) (2014).
- [22] L. V. Gambuzza, A. Buscarino, S. Chossari, L. Fortuna, R. Meucci, and M. Frasca, *Phys. Rev. E* **90**, 032905 (2014).
- [23] S. Majhi, B. K. Bera, D. Ghosh, and M. Perc, *Phys. Life Rev.* **28**, 100 (2019).
- [24] Z. Wang and Z. Liu, *Front. Physiol.* **11**, 724 (2020).
- [25] Y. Duguet and Y. L. Maistrenko, *Chaos* **29**, 121103 (2019).
- [26] K. Kawase and N. Uchida, [arXiv:1907.07285](https://arxiv.org/abs/1907.07285).
- [27] K. A. Takeuchi, M. Kuroda, H. Chaté, and M. Sano, *Phys. Rev. Lett.* **99**, 234503 (2007).
- [28] M. Sano and K. Tamai, *Nat. Phys.* **12**, 249 (2016).
- [29] G. Lemoult, L. Shi, K. Avila, S. V. Jalikop, M. Avila, and B. Hof, *Nat. Phys.* **12**, 254 (2016).
- [30] D. A. Wiley, S. H. Strogatz, and M. Girvan, *Chaos* **16**, 015103 (2006).
- [31] M. Wolfrum and O. E. Omel'chenko, *Phys. Rev. E* **84**, 015201(R) (2011).
- [32] O. E. Omel'chenko, M. Wolfrum, S. Yanchuk, Y. L. Maistrenko, and O. Sudakov, *Phys. Rev. E* **85**, 036210 (2012).
- [33] T. Girnyk, M. Hasler, and Y. Maistrenko, *Chaos* **22**, 013114 (2012).
- [34] Y. L. Maistrenko, A. Vasylenko, O. Sudakov, R. Levchenko, and V. L. Maistrenko, *Int. J. Bifurcation Chaos Appl. Sci. Eng.* **24**, 1440014 (2014).
- [35] H. Hinrichsen, *Phys. Rev. E* **55**, 219 (1997).
- [36] H. Hinrichsen, *Adv. Phys.* **49**, 815 (2000).
- [37] A. Mihara and R. O. Medrano-T, *Nonlinear Dyn.* **98**, 539 (2019).
- [38] The incoherent fraction is introduced in Refs. [25,26] and the space-time correlation function in Ref. [26] to characterize the transition behavior for $\alpha < 1/2$. We modify their definitions noting that the twisted and incoherent states are distinguished by $1 - s(x, t)^2 = 0, 1$.